A Transferrable Shell-Based Magnetic Flux Density Distribution Model for a Magnetic Proximity Detection System

Jingcheng Li, Ph.D., Jacob Carr, Adam Smith, Joseph Waynert, Ph.D.
National Institute for Occupational Safety and Health
626 Cochrans Mill Road
Pittsburgh, PA 15236, USA
Jingcheng.li@cdc.hhs.gov, Jacob.carr@cdc.hhs.gov, Adam.smith@cdc.hhs.gov, Joseph.waynert@cdc.hhs.gov

***Abstract* – A magnetic proximity detection system relies on magnetic flux density measurement to determine the position of a worker relative to a mobile mining machine. It is desirable for the magnetic flux density distribution to be automatically adjustable to conform to the protection requirements for the different types of machines and working environments. In support of the development of an automatic field distribution adjustment process, we developed a transferrable magnetic flux density distribution model. The transferrable model can also be used to control and stabilize the field against field drift to enhance system performance.**

***Index Terms*—Electromagnetic modeling, ferrite devices, magnetic field measurement, magnetic flux density, near-field radiation pattern, transfer function, vehicle safety.**

I. INTRODUCTION

Magnetic proximity detection systems are increasingly used in underground coal mines to protect miners from being pinned and struck by mining machines [1]-[3]. Since 1984, 37 fatal accidents have been reported in the United States in which a miner was pinned or struck by a continuous mining machine (CMM) [4]. To address this problem, the Mine Safety and Health Administration published a proposed regulation that would require a proximity detection system on all CMMs except full face CMMs [5].

A magnetic proximity detection system is typically composed of one or more ferrite-cored magnetic field generators mounted on a CMM to generate a magnetic field covering the space around the machine. The system relies on a magnetic flux density (*B*) measurement from a sensing device (a personal alarm device, or PAD) worn by a worker to determine the location of the worker relative to the machine. Magnetic proximity detection systems typically operate at a fixed frequency around 100 kHz.

A three-zone system is generally used to monitor the safety location of a worker. The closest area to the machine is called the stopping zone, the next closest is called the warning zone, and the zone beyond the warning zone is the safe zone [1]-[3]. The shape and width of the zones are generally set according to mutually agreed upon safety requirements which can vary from machine to machine. A magnetic field distribution model along with a *B* measurement is used to determine the zone location of a worker. Triangulation can be used with a multi-generator system. In the multi-generator system, the *B* measurements from two or more generators at a single point (the PAD) are used to calculate the position of a worker relative to the machine based on the *B*-distributions, and hence the zone location. Maintaining a steady magnetic field for a proximity detection system is critical to the system accuracy.

A proximity system needs to be calibrated and initialized before operating. In that process, the magnetic field distribution of each generator needs to be adjusted according to the zone's shape and width requirements. The resulting field distribution from multiple generators must be appropriately adjusted to provide overlapping coverage from the generators. In addition, the *B*-distribution needs to be monitored and periodically adjusted to maintain the system accuracy. A manual *B*-distribution measurement and adjustment for a system in an underground coal mine can be a difficult task because of the space restrictions of an entry (tunnel). Maneuvering a 15-m 50-ton CMM to make space for manual initialization or calibration of a proximity detection system can be difficult and unsafe. In this paper, we present a transferrable *B*-distribution model that provides a method to automatically and safely adjust the magnetic field to a desirable *B*-distribution by varying the field control variable — in this case the current — in the transferrable model (or field-variant model) at a given operating frequency.

We build on previous work of a field-invariant model [6]-[9] in which the *B* field distribution from a generator was described in terms of magnetic shells which are surfaces of revolution that enclose the generator. Each shell represents a surface of constant *B* field magnitude. A shell function is an analytical expression for the magnetic surface. Shells are different in shape and size depending on the distance to the generator. The shell-based model uses *B* shells to characterize the near-field magnetic distribution patterns of a ferrite-cored magnetic radiator.

We developed a transferrable shell-based magnetic flux density distribution model for ferrite-cored magnetic field generators from the field-invariant model introduced in [6]-[9], which is only valid to determine a shell function for a fixed current supplied to the generator. A transferrable model

is, however, valid to correctly determine a shell function over a range of current supplied to the generator.

II. The Field-Invariant *B*-Distribution Model

The transferrable shell-based *B*-distribution model was developed from its field-invariant single-frequency counterpart introduced in [6]-[9]. Expression (1) is the general three-dimensional (3-D) form of the shells in the field-invariant model. A shell function from the model can be expressed either in directional cosine coordinates (1*a*) or Cartesian coordinates (1*b*). The coordinate systems are shown in Fig. 1. Expression (2) is the two-dimensional (2-D) representation of the model. Both polar and Cartesian coordinate representations for a 2-D shell are given in Fig. 2. In both (1) and (2), c_a, d_a, c_b, and d_b are constants that completely define the steady field distribution; B is a magnetic flux density measurement; a the shell shape parameter; and b the shell size parameter. With a given B measurement, the shell parameters a and b completely define a shell's size and shape. The a and b values can be obtained from either (1*c*) and (1*d*) in (1), or from (2*d*) and (2*e*) in (2). Then the corresponding 3-D shell functions can be obtained in (1*a*) and (1*b*) and the 2-D shell function in (2*a*). Consequently, the coordinates of every point on the shell can be determined. Expressions (1) and (2) indicate that no two shells have the same shape or pattern because no two values of B result in the same values for a and b. Three representative shells from one set of our measurements are given in Fig. 3 to show the differences among the *B* shells.

$$
\begin{cases}
shell(\rho,\alpha,\beta,\gamma|B) or\ shell(x,y,z|B) = \\
\rho = a(cos^2\alpha - cos^2\beta - cos^2\gamma) + b \qquad (1a) \\
0 \le \alpha,\beta,\gamma \le \pi \\
or \\
(x^2+y^2+z^2)^{\frac{1}{2}} = a\left(\dfrac{x^2-y^2-z^2}{x^2+y^2+z^2}\right) + b \qquad (1b) \\
a + b \ge \dfrac{L}{2},\ L: length\ of\ ferrite\ core \\
a = c_a B^{-d_a} \qquad (1c) \\
b = c_b B^{-d_b} \qquad (1d) \\
B > 0, magnetic\ flux\ density
\end{cases}
\tag{1}
$$

The constants c_a, d_a, c_b, and d_b are unique for a magnetic generator of a given core length, coil windings, and current, and need to be determined before (1) and (2) can be used. The method and procedures to determine their values from measurement data are given in [6]. Their values are the same for both 3-D and 2-D models because of the field symmetry. We present our development work using the 2-D model only in this paper for simplicity. All processes described for the 2-D model apply equally to the 3-D model.

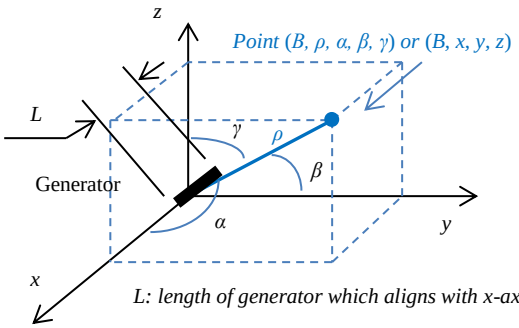

Fig. 1. Spatial coordinate systems for 3-D *B*-distribution model

$$
\begin{cases}
shell(\rho,\alpha|B)\ or\ shell(x,y|B) = \\
\rho = a\cdot cos(2\alpha) + b \qquad (2a) \\
a + b \ge L/2,\ L: ferrite\ core\ length \\
0 \le \alpha < 2\pi \\
x = \rho\cdot cos(\alpha) \qquad (2b) \\
y = \rho\cdot sin(\alpha) \qquad (2c) \\
a = c_a B^{-d_a} \qquad (2d) \\
b = c_b B^{-d_b} \qquad (2e) \\
B \ge 0
\end{cases}
\tag{2}
$$

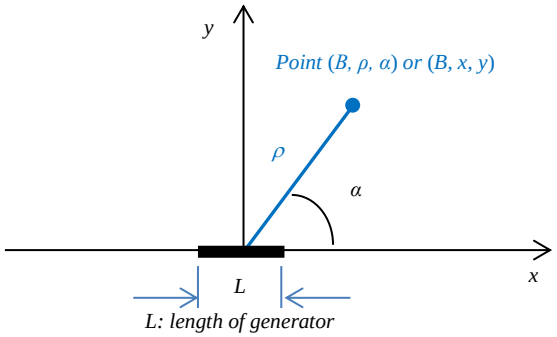

Fig. 2. Planar coordinate systems for 2-D *B*-distribution model

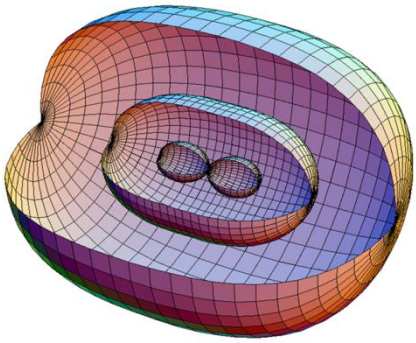

Fig. 3. Three 3-D shells from measurement data (generator in center)

A. A 2-D Field-Invariant B-Distribution Model

A 2-D field-invariant *B*-distribution model from measurement data is given in this section. The model will be, as a baseline model, converted to a transferrable model in a later section. The baseline model is for a generator with a coil

of 130 turns on a ferrite core of 25.4-mm x 25.4-mm x 304.8-mm. The ferrite is MN60-2573-970-07 (permeability of 6500 H/m). The current supplied to the generator is 480.343 mA at a frequency of 73 kHz — a typical frequency for some proximity detection systems. The *B* measurements are in milli-Gauss (mG),

With the procedures given in [6], the field constants were obtained from the measurements at 495 individual points on 16 shells with each shell having 33 measurement points. Figs. 4 and 5 show the modeling results for the constants: c_a =117.82, d_a = 0.132, c_b = 1703.9, and d_b = 0.336. As seen in Figs 4 and 5, the values of the correlation coefficients, R^2, indicate that the least squares fitting is fairly accurate. Fig. 6 provides representative plots comparing two sample modeled half shells against their measurements. The 2-D analytical form of this field-invariant *B*-distribution model is given in (3), which can be considered as one instance from an infinite number of *B*-distribution models of this generator with each having a different current. We will convert this baseline model to a transferrable *B*-distribution model in a later section.

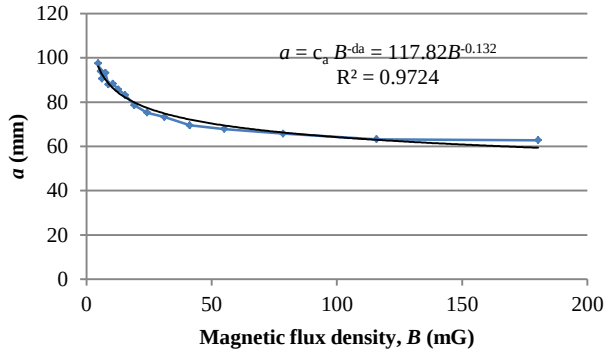

Fig. 4. Field constants c_a and d_a for the field shape parameter *a* modeled from the measurement data

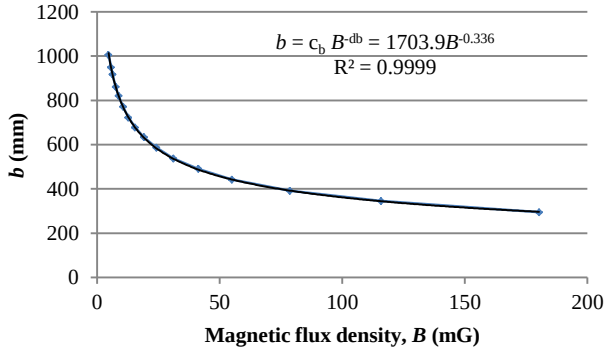

Fig. 5. Field constants c_b and d_b for the field size parameter *b* modeled from measurement data

III. TRANSFERABLE *B*-DISTRIBUTION MODEL

We will first show that the *B*-distribution pattern is an inherent property and separable from *B*-values for a generator. The separability between the *B*-distribution pattern and an individual *B*-value for the magnetic field is the foundation for attaining a transferrable *B*-distribution model. A transferrable model along with the transfer function obtained from experimental measurements is then given.

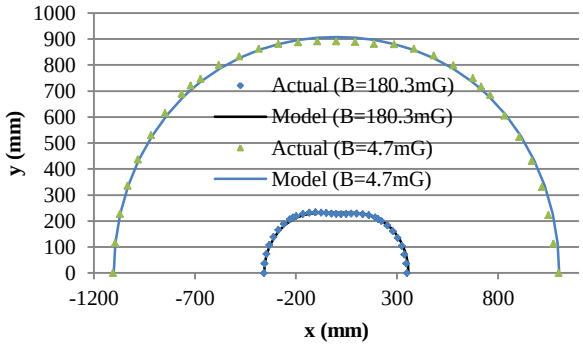

Fig.6. Measurements and the models for two half shells

$$shell(\rho,\alpha|B)\ or\ shell(x,y|B) = \begin{cases} \rho = a\cdot cos(2\alpha)+b \quad (mm) & (3a) \\ a+b \geq 152.4\ mm & \\ 0 \leq \alpha < 2\pi & \\ x = \rho\cdot cos(\alpha) \quad (mm) & (3b) \\ y = \rho\cdot sin(\alpha) \quad (mm) & (3c) \\ a = 117.82B^{-0.132} \quad (mm) & (3d) \\ b = 1{,}703.9B^{-0.336} \quad (mm) & (3e) \\ B \geq 0,\ in\ mG & \end{cases} \tag{3}$$

A. *Separation between B-Distribution Pattern and B-Value*

It is known from antenna theory that each type of antenna has its own radiation pattern in the far field. The radiation pattern is independent of the exciting source because of the absence of field exciting sources, such as voltage or current, in the antenna radiation expression. Antenna theory also shows that an antenna's far field radiation pattern is dependent on the antenna's basic geometrical shape, but not distance from the sources. The magnetic generator for proximity detection systems is actually one type of loop antenna. We will show that a generator has a unique distance-dependent magnetic distribution pattern, which is also independent of its exciting source of current. We call this the *B*/*I*-distribution pattern. The separability of the distribution pattern and the exciting source permits us to separate the measurement or calculation of *B* values at a given current from the *B*/*I*-distribution pattern, which is again unique for a given generator. We will show how the *B*/*I* distribution is related to our shell-based distribution.

The Biot-Savart law can be used to estimate the *B*-value in the vicinity of a coil without charge piling up anywhere in it as shown in Fig. 7 using a differential or integral formula as given in (4) and (5) [10]-[12], where *I* is a steady current flowing through the coil, $d\boldsymbol{l}$ is a vector quantity for an infinitesimal segment of the coil wire, and $\boldsymbol{r}$ is the vector distance from the wire segment to an arbitrary field point *P*. The cross product, $d\boldsymbol{l} \times \boldsymbol{r}$, determines both the direction and

the magnitude of component $d\boldsymbol{B}(\boldsymbol{r})$. The integral of $d\boldsymbol{B}(\boldsymbol{r})$ over the entire length of the coil wire yields both the magnitude and direction for $\boldsymbol{B}$ at P.

The steady current I in (4) and (5) can be considered a constant, and be moved to the left side of (5) resulting in (6) after taking the absolute values on both sides. The left side of (6) is the ratio of the magnitude of B to the field exciting source I. Clearly, the integral part of the right side of (6) should always yield a constant vector for a given point P regardless of changes of B and I. This is due to the fact that all segments $d\boldsymbol{l}$ and distances $\boldsymbol{r}$ in the integral are determined by the geometry of the coil and by the position of the point P relative to the coil. A constant vector has a constant magnitude and a fixed direction. The entire right side of (6) then yields a scalar constant for a constant permeability μ_0 as the absolute operation on the integral results in the magnitude only. Expression (6) indicates that the magnitude of B can change proportionally with I at a given point, and the B/I ratio is determined by the coil geometry and location of the point, not the exciting source of I. This suggests that there is only one unique shell that passes through any given point P and that shell is specified by the ratio of B/I. Conversely, a given ratio of B/I identifies a unique shell. This also indicates that the near-field distribution pattern is an inherent property of a coil in a medium with a uniform permeability.

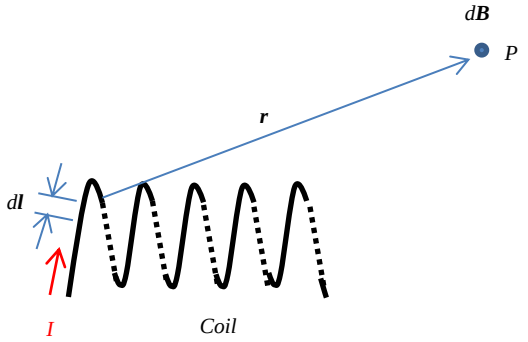

Fig. 7. Determination of magnetic flux density at a point in the vicinity of a coil

$$d\boldsymbol{B}(\boldsymbol{r}) = \frac{\mu_0}{4\pi}\frac{I\, d\boldsymbol{l}\times\hat{\boldsymbol{r}}}{|\boldsymbol{r}|^2}, \qquad \hat{\mathbf{r}}: unit\ vector \tag{4}$$

$$\boldsymbol{B} = \int_L d\boldsymbol{B}(\boldsymbol{r}) = \int_L \frac{\mu_0}{4\pi}\frac{I\, d\boldsymbol{l}\times\hat{\mathbf{r}}}{|\boldsymbol{r}|^2} = \frac{\mu_0 I}{4\pi}\int_L \frac{d\boldsymbol{l}\times\hat{\boldsymbol{r}}}{|\boldsymbol{r}|^2} \tag{5}$$

$$\frac{B}{I} = \frac{|\boldsymbol{B}|}{I} = \frac{\mu_0}{4\pi}\left|\int_L \frac{d\boldsymbol{l}\times\hat{\boldsymbol{r}}}{|\boldsymbol{r}|^2}\right| = a\ constant\ at\ a\ point \tag{6}$$

B. *Transferrable B-Distribution Model*

The B/I relationship given in (6) permits us to establish a transfer function to map a new B resulting from a changed I to its correct shell. Expression (6) can be rewritten in the form shown in (7), where C is a constant at a given location. With the current change from I to $I + \Delta I$, the corresponding change in B, $B + \Delta B$ can be determined by (8). Dividing both sides of (7) by (8) yields (9), which indicates that the proportional change in B is the same as the proportional change in the current. Letting $B_b = B$ the base magnetic flux density, $B_c = B_b + \Delta B$ the changed magnetic flux density, $I_b = I$ the base current, and $I_c = I_b + \Delta I$ the changed current in (9) yields (10), Expression (10) can be changed to (11), where τ is defined as the transfer function. Because $B_b/I_b = B_c/I_c$ and they define the same shell, the shell for the B_c can be found by finding the shell for B_b through the transfer function. The transfer function τ enables us to convert the current-specific field-invariant baseline model (2) to a general transferrable or field-variant model (12).

One concern is that the ferrite core may introduce a nonlinearity into the B/I relationship. The primary purpose of the ferrite core for the coil is to increase the magnetic flux in the coil and the effective length of the coil, causing an increase in the distributed magnetic field around the coil. The core also introduces its own magnetic characteristics into the magnetic field, which can complicate the transfer function. Among the magnetic characteristics of the ferrite is the B-H relationship at a given frequency, where H is magnetic field strength. A B-H relationship of a ferrite material is often given as a plot based on experimental measurements, not a simple formulated equation. We propose a method to experimentally find the impact of the ferrite magnetic characteristics, including its B-H relationship, on a transfer function.

$$B = C \cdot I \tag{7}$$

$$B + \Delta B = C(I + \Delta I) \tag{8}$$

$$\frac{B}{B+\Delta B} = \frac{C\cdot I}{C(I+\Delta I)} = \frac{I}{I+\Delta I} \tag{9}$$

$$\frac{B_b}{B_c} = \frac{I_b}{I_c} \tag{10}$$

$$B_b = \frac{I_b}{I_c}\cdot B_c = \tau \cdot B_c, \qquad where\ \ \tau = \frac{I_b}{I_c} \tag{11}$$

$$shell(\rho,\alpha|B_c)\ or\ shell(x,y|B_c) = \begin{cases} \rho = a\cdot cos(2\alpha) + b & (12a) \\ a + b \geq L/2,\ \ L: fettie\ core\ length & \\ 0 \leq \alpha \leq 2\pi & \\ x = \rho\cdot cos(\alpha) & (12b) \\ y = \rho\cdot sin(\alpha) & (12c) \\ a = c_a(B_b)^{-d_a} = c_a(\tau B_c)^{-d_a} & (12d) \\ b = c_b(B_b)^{-d_b} = c_b(\tau B_c)^{-d_b} & (12e) \\ B_c \geq 0,\ changed\ flux\ density & \\ \tau = I_b/I_c & (12f) \\ I_b: the\ base\ current\ for\ the\ shell, & \\ and\ \ I_c: changed\ current. & \end{cases} \tag{12}$$

C. *A Transfer function for Ferrite-Cored Coil*

To attain a transfer function τ for a ferrite-cored coil or generator, we conducted an experiment to obtain the B/I relationship. Fig. 8 illustrates the experimental setup for acquisition of measurements of B and I from a generator. The generator and an isotropic magnetic flux density probe

(which is from the IDR 200 VLF Gauss meter in our experiment) are placed on a flat wooden table. The probe provides a reading of the magnetic field magnitude. The probe is at an arbitrary but fixed location relative to the generator during the data acquisition process. The capacitor *C* connected with the generator forms a circuit to match the output impedance of the amplifier at frequency of 73 kHz. The current to the generator is measured with the current probe, which is an AH BCP-522.

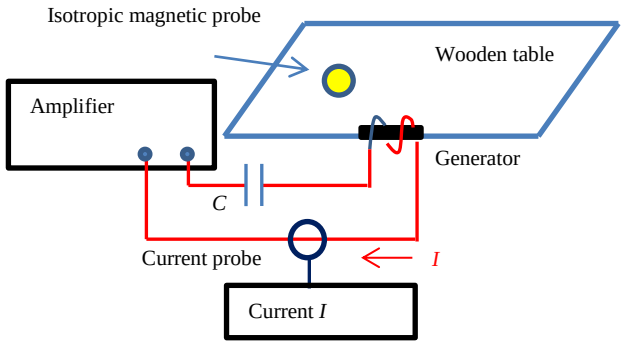

Fig. 8. The basic setup for *B-I* measurements

Fig. 9 provides a representative plot of the *B-I* measurements at a particular location for the generator introduced in Section II, and the least squares linear fit equation, which can be considered as an empirical *B*/*I* model, and is given again in (13). A generalized *B*/*I* relationship for a ferrite-cored coil is then given in (14). The corresponding ratio change in *B* due to a changed $I+\Delta I$ is given in (15). The ratio of the base flux density B_b to the changed flux density $B_c = B_b+\Delta B$ can be rewritten in (16), and is clearly not equal to the ratio of *I*'s as predicted by (9). From (16), we then obtain (17) and the transfer function (18), which is evidently different from (11). The constant Q in (14) to (18) is produced by the non-zero intercept in the fitting equation to the magnetic characteristics of the ferrite core. Although the transfer function (18) is more accurate for a ferrite-cored coil, the equality (11) can still hold approximately for a small constant term Q, and large supply currents as shown in the next example. Conducting an experiment to attain an accurate transfer function for every generator (i.e. determining the value of Q) is often not practically feasible.

It is worth pointing out that the constant C in (7) is the result of the spatial vector integral of the right side of (6) for a given point near the coil. Because values of the integral variables vary with the location of the point, the values of C vary with the position, indicating that the value of C is a location-dependent constant. The value of the constant C in (15) is, in addition, determined by the geometry and magnetic characteristics of a given ferrite-cored coil, indicating that the value of C is, in addition, a core-geometry-and-magnetic-characteristics-dependent constant. However, the Cs disappear in both transfer functions (11) and (18), indicating that these transfer functions are no longer location- and core-geometry-and-magnetic-characteristic-dependent functions, but global functions for a given generator. This explains why the magnetic probe can be placed at an arbitrary location for *B-I* measurements to attain the transfer function, and why a single transfer function is valid for the whole transferrable model.

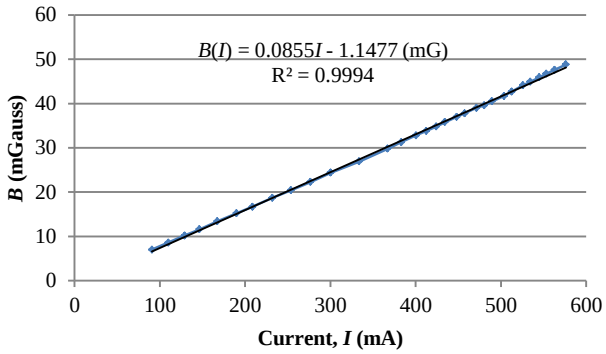

Fig. 9. Measurements and the linear fit of the magnetic flux density versus the current to the generator

$$B(I) = 0.0855I - 1.1477\ (mG) \tag{13}$$

$$B(I) = P \cdot I + Q,\ \ P\ \&\ Q\text{: constant} \tag{14}$$

$$\frac{B}{B+\Delta B} = \frac{C(PI+Q)}{C[P(I+\Delta I)+Q]} = \frac{C(PI+Q)}{C(PI+Q)+C\Delta I} \tag{15}$$

$$\frac{B}{B+\Delta B} = \frac{B_b}{B_c} = \frac{C(PI_b+Q)}{C(PI_c+Q)} = \frac{PI_b+Q}{PI_c+Q} \tag{16}$$

$$B_b = \frac{PI_b+Q}{PI_c+Q}\cdot B_c = \tau \cdot B_c, \qquad where\ \tau = \frac{PI_b+Q}{PI_c+Q} \tag{17}$$

$$\tau = \frac{PI_b+Q}{PI_c+Q}, for\ ferrite\ cored\ generator \tag{18}$$

D. A Test for the Transferrable Model

We converted the field-invariant *B*-distribution model (3) to a transferrable model (19) with the use of transfer function (11) and base current I_b = 480.343 mA and tested it. We used the transfer function (11) instead of the more accurate (18) to demonstrate that the simple transfer function is reasonably accurate for a large generator current and a small Q.

$$shell(\rho,\alpha|B_c)\ or\ shell(x,y|B_c) = \begin{cases} \rho = a\cdot cos(2\alpha)+b & (19a) \\ a+b \geq 152.4\ mm \\ 0 \leq \alpha < 2\pi \\ x = \rho\cdot cos(\alpha) & (19b) \\ y = \rho\cdot sin(\alpha) & (19c) \\ a = 117.82(\tau B_c)^{-0.132}\ mm & (19d) \\ b = 1{,}703.9(\tau B_c)^{-0.336}\ mm & (19e) \\ B_c \geq 0,\ changed\ flux\ density\ in\ mG \\ \tau = (480.343\ mA)/I_c & (19f) \\ I_c\text{: a changed current in mA.} \end{cases} \tag{19}$$

The first test was conducted with the current increased to I_c = 544.574 *mA* — a 13.37% increase from the base current. The transfer function in (19) was then τ = (480.343/544.574) = 0.8821. Note that (19*d*) and (19*e*) use the same constants given in (3*d*) and (3*e*) which are based on measurements using I_b. The measurement-based shell function given in (20) is based on the shell measurements with an arbitrarily selected B_c = 7.8 mG and I_c as given. The shell function given in (21) is from the transferred model (19). The two results plotted in half shells are compared in Fig. 10 against the measurements. The shell in diamonds is the measurements; the "measurement-based" shell in the dashed curve is the shell modeled from the measurements at I_c; the "transferred" shell (solid line) is the shell from the transferrable model (19). The absolute average difference of the amplitudes ρ between the shells of "transferred" and "measurement-based" is 0.43 mm; the relative difference to ρ is 0.05%, while the absolute maximum difference is 0.76 mm, and the relative maximum difference is 0.08%.

$$\rho = 92.02\cos(2\alpha) + 891.36 \quad (mm) \qquad (20)$$

$$\rho = 91.34\,cos(2\alpha) + 891.28 \quad (mm) \qquad (21)$$

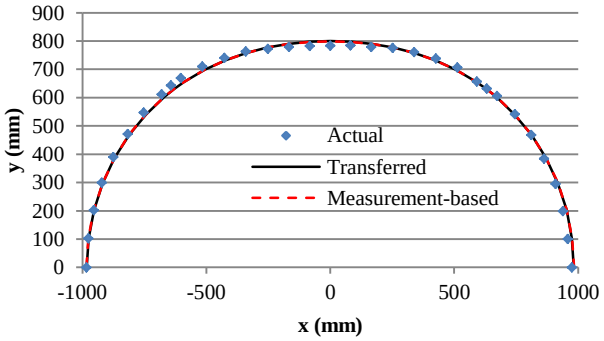

Fig. 10. Comparison of the measurements of a shell with B_c = 7.8 mG, the measurement-based shell model calculated based on the measurements, and the shell from the transferred model of (19)

The second test was with the current reduced to I_c = 400.447 *mA* — a 16.63% decrease from the base current. The transfer function was then τ = 480.343/400.447 = 1.120. The shell measurements were made with B_c = 38.8 mG. The measurement-based shell function is given in (22). The shell function from the transferred model (19) is given in (23). The comparison of these shells against the measurements can be seen in Fig. 11. The absolute average difference of ρ between "transferred" and "measurement-based" is 2.30 mm, and the relative difference to ρ is 0.46%.

To further compare the transferred model using (19*f*) (or (11)) to the one using the transfer function (18), where P = 0.0855 and Q = -1.1477, we also provide the transferred shell function with use of (18) as given in (24). The absolute average difference of $|\rho|$ between the shell functions (22) and (24) reduces to 1.64 mm, and the relative difference reduces to 0.33%. This then suggests that the transfer function (18) is slightly better than (11) as expected.

$$\rho = 68.83\cos(2\alpha) + 466.64 \quad (mm) \qquad (22)$$

$$\rho = 70.97cos(2\alpha) + 468.87 \quad (mm) \qquad (23)$$

$$\rho = 70.91cos(2\alpha) + 467.96 \quad (mm) \qquad (24)$$

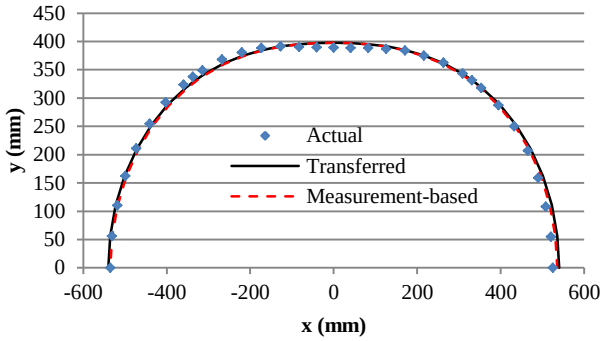

Fig. 11. Comparison of the measurements with B_c = 38.8 mG, the shell calculated based on the measurements, and the shell from the transferred shell model (22)

E. Discussion

There is no a clear cut method for selecting a transfer function between (11) and (18) for a ferrite-cored coil as demonstrated in our tests. A marginal benefit results from use of (18) when Q has a small absolute value and a generator has a large current. For a small generator current, the use of Q may reduce the error contribution to a transferred model.

Once the transferrable *B*-distribution model is ready, there is no need to obtain an additional model for every generator current. The transferrable model can considerably reduce the effort necessary to establish an initial magnetic field distribution in a calibration process or to re-adjust the distribution for a proximity detection system. The field adjustment can be made by adjusting the current to the generator. A current adjustment process could also be done remotely through a communication network, reducing exposure of engineers and technicians to the hazardous machine working environment.

A transferrable model can also find applications in automatic magnetic field control against field drift due to current fluctuation. The generator current can be used as a control variable in a feedback control system to dynamically correct the field drift to improve the system dynamical accuracy. Or the drift can be evaluated based on the current and field relationship, and dynamically compensated in PAD position calculation. Both approaches can result in an increased accuracy of the proximity detection system.

In addition, the transferrable model lays the foundation for a quantitative study of the influence of steel and metal parts of a machine on the magnetic field distribution of a proximity detection system. The baseline model of a transferrable model can be considered as the model providing the generic near-field distribution pattern. Any distribution pattern change due to the influence of nearby steel and metal parts

can be identified, quantitatively analyzed, and modeled [13]. This can lead to a magnetic field model with the compensation of the environment factors possibly resulting in a higher adaptability of the system to different operating environments.

Moreover, the transferrable model can find an application in the computer simulation of magnetic field coverage analysis and design for a multi-generator system. The simulation provides a method to estimate the field coverage of each generator at a current on a machine, and determine an operating current of each generator for a desirable overall field coverage of the system. It is a not only a time- and effort-saving method but also a safer method for field coverage design.

IV. Summary

In this paper, we show that a magnetic field generator of a magnetic proximity detection system has a near-field distribution pattern, *B*/*I*-distribution pattern, which is independent of the magnetic flux density and exciting current. The *B*/*I*-field distribution can be envisioned as a collection of nested shells, with each of those surfaces representing a constant value of *B*/*I*. The *B*/*I* distribution is unique for a given generator. We use this property to build a transferrable magnetic flux density distribution model. A current-specific or field-invariant *B*-distribution model needs to be obtained from measurements of *B* at a given current *I* as one objectification of the *B*/*I*-distribution model before being transferred to the transferrable model by introducing a transfer function. We introduce a method to obtain the transfer function for a ferrite-cored generator. The transferrable model is applicable to a wide range of the exciting current, improving upon the field-invariant model which is applicable to a single fixed current only. We also show the influence of the magnetic characteristics of the ferrite core on the transfer function. The transferrable model can find applications in advanced technology development for a magnetic proximity detection system — from system calibration, automatic field adjustment and control to the system simulation. The transferrable model also lays a foundation for a quantitative evaluation and modeling of the influence of the steel and other metal parts of the machine on the magnetic field. It may find applications in a general near-field radiation study of a ferrite-cored rod antenna as well.

Disclaimer

The findings and conclusions in this report are those of authors and do not necessarily represent the views of the National Institute for Occupational Safety and Health. The mention of any company or product does not constitute an endorsement by NIOSH.

Acknowledgment

The authors gratefully acknowledge the contributions of Mr. Joseph P. DuCarme, Dr. Christopher C. Jobes, Mr. Timothy J. Lutz, Mr. Miguel A. Reyes, and Mr. Jeffrey A. Yonkey during the time of the experimental setup. The authors also want to show their great appreciation to Mr. Peter G. Kovalchik for his firm support of this work.

References

[1] W. H. Schiffbauer, "Active Proximity Warning System for Surface and Underground Mining Applications," *Mining Engineering*, Dec. 01. 2002.

[2] D. Chirdon, "MSHA Proximity Detection," http://www.msha.gov/Accident_Prevention/NewTechnologies/ProximityDetection/Proximity%20Detection%Pager.pdf.

[3] T. Ruff, "Overview of Proximity Warning and Technologies and Approaches," presentation at NIOSH Workshop on Proximity Warning Systems for Mining Equipment, Charleston, WV, September. 15, 2010, http://www.cdc.gov/niosh/mining/UserFiles/workshops/ proximityworkshop2010/Ruff-NIOSH-PDWorkshop2010-508.pdf.

[4] C. Huntsley, "Remote Controlled Continuous Mining Machine Fatal Accident Analysis Report of Victim's Physical Location with Respect to the Machine." December 23, 2011. Retrieved from http://www.msha.gov/webcasts/Coal2005/Fatal%20Accident%20Summary.pdf on 5/17/2012.

[5] Mine Safety and Health Administration. "Proximity Detection Systems for Continuous Mining Machines in Underground Coal Mines." Notice of Proposed Rule Making. Federal Register Volume 76, Number 169. August 31, 2011. pp. 54163–54179.

[6] J. Li, J. Carr, C. Jobes, "A shell-based magnetic field model for magnetic proximity detection systems," *Safety Science*, Vol. 50, Issue 3, March 2012, pp. 463-47.

[7] J. Carr, C. Jobes, J. Li, "Development of a method to detect operator location using electromagnetic proximity detection," conference publication, IEEE International Workshop on Robotic and Sensors, Oct. 15-16, 2010, Phoenix, AZ, USA.

[8] J. Li, J. Carr, C. Jobes, "Modeling of the magnetic field around a ferrite-cored generator in a proximity detection system," presented at 14th Conference on Electromagnetic Field Computation, May 9-12, Chicago, IL, USA.

[9] J. Li, C. Jobes, and J. Carr, "Comparison of magnetic field distribution models for a magnetic proximity detection system," IEEE Transactions on Industry Applications, May/June Issue, 2013. Vol. 49, pp. 1171-1176.

[10] D. Griffiths, "Introduction to Electrodynamics,",3rd ed.. Prentice-Hall, Inc., Uooer Saddle River, New Jersey 07458, pp.215-220.

[11] "Modular 19: Sources of Magnetic Fields: Biot-Savart Law," MIT OpenCource, available: http://ocw.mit.edu/courses/physics/8-02sc-physics-ii-electricity-and-magnetism-fall-2010/creating-magnetic-fields/biot-savart-law/MIT8_02SC_lectureslides19.pdf.

[12] "Chapter 9: Sources of Magnetic Fields," MIT OpenCource, available: http://web.mit.edu/viz/EM/visualizations/notes/modules/guide09_revised.pdf.

[13] J. Li, J. Carr, J. Waynert, and P. Kovalchik, "Environmental Impact on the magnetic field distribution of Magnetic Proximity Detection System in an Underground Coal Mine," *Journal of Electromagnetic Waves and Applications*, 2013 Vol. 27, Number 18, pp. 2416-2419.

OCTOBER 5-9, 2014

IAS ANNUAL MEETING 201

2014 IEEE Industry Applications Society ANNUAL MEETING

SHERATON VANCOUVER WALL CENTRE HOTEL
VANCOUVER, BRITISH COLUMBIA

IEEE